ISSN 2070-0482, Mathematical Models and Computer Simulations, 2010, Vol. 2, No. 3, pp. 396–405. © Pleiades Publishing, Ltd., 2010.
Original Russian Text © V.I. Mazhukin, A.V. Mazhukin, M.G. Lobok, 2009, published in Matematicheskoe Modelirovanie, 2009, Vol. 21, No. 11, pp. 99–112.

Mathematical Modeling of Dynamics of Fast Phase Transitions and Overheated Metastable States During Nano- and Femtosecond Laser Treatment of Metal Targets

V. I. Mazhukin, A. V. Mazhukin, and M. G. Lobok

Institute of Mathematical Modeling, Russian Academy of Sciences, 4a Miusskaya pl., Moscow, 125047 Russia

e-mail: immras@orc.ru

Received November 20, 2008

Abstract—For a mathematical description of pulsed laser heating, melting, and evaporation of an aluminium target in an ambient atmosphere, a one dimensional, multifront hydrodynamic Stephan problem was used, written for both phases (liquid and solid). On the boundary of solid and gaseous forms, the Stephan problem is combined with radiation gas-dynamic equations, with thermal conductivity, and describes processes in the evaporated material and surrounding gas. For the numerical solution, finite difference method of dynamic adaptation, which gives an opportunity of explicitly tracking interphase boundaries and shock waves, was applied. As a result, in the process of the solution, the problem had 6 computational regions and 7 boundaries, 6 of them were moving, including 2 shock waves and one free boundary in the atmosphere. We used this model to calculate the pulsed laser interaction with an aluminium target with the following parameters: $\lambda = 0.8$ μm, $\tau = 10^{-8}$–10^{-15} s, and $G_0 = 10^{-9}$–10^{-16} W/cm^2. Modeling revealed that in the case of long ~1 ns pulses, most of the energy is spent on melting and heating the liquid. The depth of the molten pool depth constitutes about 1.2 μm. In the case of femtosecond pulses, most of the energy is spent on heating the solid body and the formation of shock waves in it. The depth of the molten pool does not exceed 0.03 μm. Even though the evaporated layers were of almost the same thickness. For nanosecond laser pulses with fluence J less than 30 J/cm^2, there is no plasma formation in the evaporated material. For the same fluence of femtosecond laser pulses, plasma is formed after the pulses and is thermal by nature.

DOI: 10.1134/S2070048210030130

INTRODUCTION

The most important and influential parameters in the laser processing of materials, along with wavelength λ, are the pulse intensity G and duration τ. Two processes, the ablation of a material and plasma formation play dominating roles in laser processing [1]. In the case of plasma formation, the dynamics of these processes turns out to be interconnected [2].

The influence of high-intensity $G = 10^{15}$–10^{18} W/cm^2 lasers on solid targets is one of the ways of creating laser plasma with unique characteristics. The thin $l \sim 0.1$ μm plasma layer, forming on the surface of a solid target by an ultrastrong light field, possesses an electron temperature $T \sim 100$ eV, high density of charged particles $N_e \sim 10^{22}$–10^{23} cm^{-3} and high gradients of electrons and ions. Such a plasma is the source of strong X-ray radiation [3], [4], which is one of the reasons of great interest in it.

Pulsed laser ablation underlies a number of widely used technologies, such as drilling, cutting, micro- and nanostructuring, spraying thin films, etc. [5]. Plasma and its evolution in laser ablation-based applications in most cases play a negative role, however they may be interesting as well.

The influence of long and short pulses qualitatively differs according to the mechanisms of the conversion of laser radiation energy and the removal of matter from the radiation region. In the millisecond duration range, the main removal mechanisms are connected with hydrodynamic phenomenons: thermocapillarity, pressure, return, and others [6]. The instability of a number of processes is the distinguishing feature of hydrodynamic mechanisms [7].

It is necessary to note an important role of phase transitions—melting and evaporation—in millisecond and submillisecond ranges. Modeling [8] showed that predominance of one or the other process mostly depends on the temporal form of the pulse. If energy contribution is characterized by acceleration or process stationarity, then the evaporation process predominates and the thicknesses of molten Δ_l and evaporated Δ_{ev} matters fit the expression $\Delta_l/\Delta_{ev} \ll 1$. Melting $\Delta_l/\Delta_{ev} \gg 1$ predominates for pulses with a

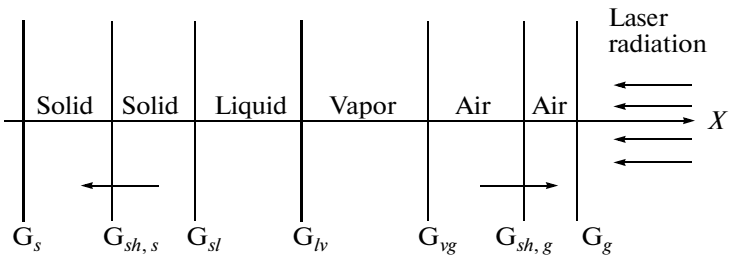

Fig. 1. Scheme of spatial phase positions.

flowing temporal profile (flowing triangle) and a temporal form without a constant component (Gaussian profile).

In the nanosecond range, the role of evaporation and laser plasma intensifies [9], [10]. In a number of modes, volumetric boiling completes surface evaporation [11].

Laser ablation in pico- and femtosecond ranges is the most unstudied. At the same time, the number of publications in this sphere have steadily grows, testifying to the great interest in the influence of high-intensity laser pulses on condensed mediums [12, 13]. Mostly, these works are devoted to experimental observations [14–16]. Far fewer works attempt to theoretically explain the fundamental phenomenona, accompanying ultrashort effect [17–19].

The main peculiarities of ultrashort effect on metals are connected with the high-speed and volumetric nature of the liberation of laser pulse energy. The high heating rate of a condensed medium is conjugated with fast phase transformations of matter, which is characterized by the transition of strong mass and energy flows through interphase boundaries. The removal of energy by the flow of matter on aggregate with the volumetric mechanism of the liberation of the energy of laser radiation promote the heating of interphase surfaces to temperatures, which significantly exceed the temperatures of melting T_{m0} and evaporation T_b. Because of the same reasons, regions of temperature maximums are formed near the irradiated surfaces in solid and liquid phases.

At the beginning, overheated metastable states were considered and fixed in the nanosecond influence range [20]. In one of the first works [21], the overheating of the solid phase by 40–110 K with respect to a temperature of T_{m0} was experimentally established via the effect on silicon of a 26-ns long laser pulse. In theoretical works [22, 23], the dynamics of overheated metastable states in superconducting silicon irradiated by pulses of nanosecond durations was studied with the help of mathematical modeling. The maximal overheating of solid phase with respect to a temperature of T_m constituted 150 K.

With the development of laser techniques, reports [24] and articles [25–27] on the observation of overheated metastable regions in pico- and femtosecond ranges of influence appeared.

Generalizing the experimental results [15] of metal drilling by ultrashort pulses, we note the following peculiarities and advantages:

—In proceeding from nano- to femtosecond durations, part of the liquid fraction decreases and the quality of the aperture increases;

—When the energy density $J \le 5$ J/cm^2 of a pico- and femtosecond laser pulse no plasma formation occurs;

—Thermal conductivity effects are negligible in the time scale of the pulse;

—The average thickness of an evaporated layer at $J \le 1$ J/cm^2 doesn't exceed 100 nm.

It is necessary to note the important role of the dynamics of complex interconnected processes in condensed and gaseous mediums in the formation of macroprocess on the whole. Thus, process dynamics is connected with heating, cooling, and phase transition in the irradiated target. Thermal conductivity and ablation define the dynamics of plasma cooling-down after the influence of a laser pulse. At the same time, studying the dynamics of processes, especially when using ultrashort pulses, is linked with almost insuperable restrictions. As a rule, experimental observations represent aftereffect results, which are insufficient for understanding why the system gets into one or another state as a result of the influence. In such conditions, the role and partial weight of mathematical modeling methods in researches sharply increases.

The given work is devoted to mathematical modeling of dynamics of phase transitions, overheated metastable states, and comparative analysis of the main characteristics of laser ablation in the nano- and femtosecond range of influence.

PROBLEM STATEMENT

Laser radiation propagates from right to left, being partially absorbed and partially reflected by the surface of the metal target (Fig. 1). Figure 1 also shows the spatial position of phases, interphase boundaries Γ_{sl}, Γ_{lv}, and shock waves $\Gamma_{sh,s}$, $\Gamma_{sh,g}$.

The problem was stated under the following assumptions and restrictions:

—Energy removal of laser radiation regarding the target grid occurs instantly;

—Phase transformations are of a thermal nature;

—Mechanisms of volumetric melting and evaporation are not considered. It is assumed that the melting front appears on the irradiated surface at the moment of reaching a temperature if T_{m0};

—Overheated metastable states behave stably during the observation.

The mathematical description and modeling of a laser ablation of a solid aluminium target into a medium with reverse pressure is performed within the framework of a one-dimensional multifrontal hydrodynamic Stephan problem, written for both solid and liquid phases. The Stephan problem is connected with the gas dynamics equation system including thermal conductivity, which describes processes in evaporated matter and a gaseous medium (air):

$$\left[\begin{array}{c} \dfrac{\partial \rho}{\partial t} + \dfrac{\partial(\rho u)}{\partial x} = 0 \\ \dfrac{\partial(\rho u)}{\partial t} + \dfrac{\partial(\rho u^2)}{\partial x} + \dfrac{\partial P}{\partial x} = 0 \\ \dfrac{\partial(\rho\varepsilon)}{\partial t} + \dfrac{\partial(\rho u\varepsilon)}{\partial x} = -\left(P\dfrac{\partial u}{\partial x} + \dfrac{\partial W_T}{\partial x} + \dfrac{\partial W_I}{\partial x} + \dfrac{\partial G}{\partial x}\right) \\ \dfrac{\partial I_\nu}{\partial x} + \kappa(h\nu, \rho, T)I_\nu = \kappa(h\nu, \rho, T)I_{\nu,eq} \\ W_\nu = \int_0^\infty\int_{-1}^{1}\mu I_\nu d\nu d\mu, \quad W_T = -\lambda(T)\dfrac{\partial T}{\partial x} \\ \dfrac{\partial G}{\partial x} - \kappa_L(\rho, T)G = 0 \\ P = P(\rho, T), \quad \varepsilon = \varepsilon(\rho, T) \end{array}\right]_k, \quad k = s, l, v, g, \tag{1}$$

$$t > 0, \quad x \in [\Gamma_s, \Gamma_{sh,s}(t)] \cup [\Gamma_{sh,s}(t), \Gamma_{sl}(t)] \cup [\Gamma_{sl}(t), \Gamma_{lv}(t)] \cup [\Gamma_{lv}(t), \Gamma_{vg}(t)]$$
$$\cup [\Gamma_{vg}(t), \Gamma_{sh,g}(t)] \cup [\Gamma_{sh,g}(t), \Gamma_g(t)].$$

The accepted denotations: ρ, u, ε, T, and P are, respectively, the density, gas-dynamic speed, internal energy, temperature, and pressure of matter; κ and I_ν are the absorption coefficient and spectral density of plasma radiation; $I_{\kappa\nu,eq}$ is the density of equilibrium radiation; κ_L and G are the absorption coefficient and density of laser radiation; and λ is the thermal conductivity coefficient. Indexes s, l, v, and g denote that the magnitudes belong to solid, liquid, vaporous, and gaseous mediums, respectively.

Figure 1 shows the spatial position of phases.

BOUNDARY CONDITIONS

1. Stationary left boundary

$$x = \Gamma_s: \; u = 0, \quad W_T = 0, \quad W_I = 0. \tag{2}$$

2. Melting-crystallization $x = \Gamma_{sl}$: on the melting boundary 3 conservation laws are formulated concerning mass, pulse, and energy, written in the coordinate system, moving at the speed of a solid phase $v_{sl} = v_{sl}^* - u_s$, where v_{sl}^* is the propagation rate of the melting-crystallization front in a fixed (laboratory) coordinate system:

$$\rho_s v_{sl} = \rho_l(u_l - u_s - v_{sl}), \tag{3}$$

$$P_s + \rho_s v_{sl}^2 = p_l + \rho_l (u_l - u_s - v_{sl})^2, \tag{4}$$

$$W_l^T - W_s^T = \rho_s v_{sl} L_m^{ne}, \tag{5}$$

where $W_s = -\lambda(T_s)\dfrac{\partial T_s}{\partial x}$, $W_l = -\lambda(T_l)\dfrac{\partial T_l}{\partial x}$, C_{ps}, C_{pl} are the heat capacities of solid and liquid phases, respectively, and $L_m^{ne} = L_m + (C_{pl} - C_{ps})(T_{sl} - T_m) + \dfrac{\rho_s + \rho_l}{\rho_s - \rho_l}\dfrac{(u_s - u_l)^2}{2}$ is nonequilibrium melting heat.

Energy conservation law (5), representing the differential condition of Stephan, is supplemented with a phenomenological condition of temperature equality on the interphase boundary

$$T_{sl} = T_s = T_l = T_m(P_s). \tag{6}$$

The melting temperature T_m was assumed to depend on pressure $T_m(P_s)$.

3. Evaporation $x = \Gamma_{lv}$: on the evaporating boundary, 3 conservation laws are formulated in the coordinate system moving at the speed of the solid phase $v_{sl} = v_{sl}^* - u_s$:

$$\rho_l v_{lv} = \rho_v (u_l - u_v + v_{lv}), \tag{7}$$

$$P_l + \rho_l v_l^2 = p_v + \rho_v (u_l - u_v + v_{lv})^2, \tag{8}$$

$$W_l^T - W_v^T = -\rho_l v_{lv} L_v^{ne}, \quad G = A(T)G_l, \quad W_v = W_v^l, \tag{9}$$

where $L_v^{ne} = L_v^e(T_l) + C_{pv}(T_b - T_{lv}) + \dfrac{\rho_l + \rho_v}{\rho_l - \rho_v}\dfrac{(u_l - u_v)^2}{2}$ is the nonequilibrium evaporation heat. Magnitudes T_v, ρ_v, and p_v are defined from the expressions on the nonequilibrium Knudsen layer by the modified Krut model [28]:

$$T_v = \alpha_T(M) T_l, \quad \rho_v = \rho_H \alpha_\rho(M), \tag{10}$$

where $\alpha_T(M)$, $\alpha_\rho(M)$ are Krut coefficients, $M = u_v/u_{sh}$ is the vapor outflow velocity in terms of Mach numbers; ρ_H, $P_H(T_l)$ are the density and pressure of saturated vapors at a temperature of T_l.

An approximately 30-μm-thin aluminium target in air at a temperature of $T_0 = 273$ K and pressure $P_0 = 1$ bar was considered as the researched matter. Values, corresponding to the solid and liquid phases of aluminium, were used as the thermalphysic parameters. Equilibrium melting temperature constitutes $T_{m,0} = 993$ K. Experimental dependence [29], approximated by the linear expression $T_m(P_s) = (T_{m,0} + kP_s)$, where $k = \partial T_m/\partial P_s = 2 \times 10^{-4}$ K/bar, was used as the function $T_m(P_s)$. The critical temperature for aluminium was assumed to be equal to $T_{cr} = 8 \times 10^3$ K. Beginning from the temperature $T = 0.85 T_{cr}$, depending on the coefficients of thermal conductivity and the absorption of laser radiation, their exponential decreasing and exponential increasing was introduced at the critical point $\lambda_{cr} = 0.01$ J/(K cm), $\kappa_{cr} = 10^3$ cm^{-1} and $C_{cr} = 10.200$ J s/(g K). A wide range of the state equation [30] is used as the state equation.

COMPUTATION ALGORITHM

Numerical solution of the differential problem (1)–(9) was performed with the help of the finite difference method with dynamic adaptation [31], which allows carrying out calculations with explicit allocation of interphase boundaries and shock waves. As a result, the number of computation domains may reach six; at the same time, the number of boundaries will be equal to seven, six of which are moving, including two shock waves and a free right boundary in the atmosphere.

MODELING RESULTS

The formulated model was applied for modeling a number of modes of the influence of laser with a wavelength of $\lambda = 0.8$ μm, Gaussian intensity distribution by time $G(t) = G_0 \exp(-(t/\tau)^2)$, duration $\tau = 10^{-8}$–10^{-15} s, and peak intensity $G_0 = 10^8$–10^{16} W/cm^2. In the temporal distribution of a laser pulse $-\infty < t <$ maximum ∞ intensity corresponds to the moment of time $t = 0$, and the moment of time $t = -4\tau$ is used as the beginning of the calculations. In the calculations, the energy density $J = G_0\tau$ changed in the range $1 \le J \le 50$ J/cm^2, and the absorptive capacity of the surface constituted $A = 10\%$.

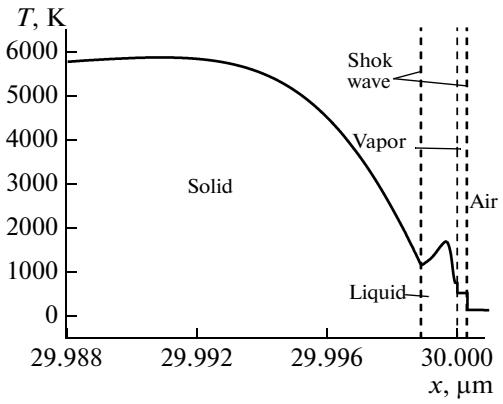

Fig. 2. Spatial profile of temperature at the moment $t = 78.5$ fs for the influence mode with $\tau = 10$ fs and $G_0 = 10^{14}$ W/cm^2.

Modeling showed that plasma in evaporated matter is formed for $J > 30$ J/cm^2 (the threshold value for plasma $J_{max} = 30$–50 J/cm^2). Since plasma slows down the evaporation process, the main attention was paid to modes before plasma formation.

Energy Liberation

Energy liberation of laser radiation in a condensed medium in a dependence on the influence mode, the thermalphysic and optic properties of the target may occur volumetrically or superficially. If the length of thermal influence $l_T = (a\tau)^{0.5}$ is much greater than the free path length $l_v = \kappa^{-1}$ of the radiation quantum $l_T \gg l_v$, where a is the thermal diffusivity coefficient, then, the absorption of laser radiation is characterized by a superficial nature. In the opposite case, absorption nature is volumetric. In modes with phase transformations, the length of thermal influence is estimated by the expression $l_T = a/v$, where v is the motion velocity of the phase front (melting, evaporation). Thus, at the velocity $v \geq (10–10^2)$ μs^{-1}, corresponding to typical values of phase transition speeds in the nanosecond range even in metal targets, modes of volumetric radiation energy liberation, $\alpha\kappa/v \leq 1$, are achieved.

According to these elementary estimations, the nanosecond mode of influence on metals, at which a change of the superficial absorption mechanism by volumetric occurs, is transitional. In the pico- and femtosecond range, absorption is wittingly volumetric, as $l_T \ll l_v$. Thus, in the influence modes under consideration, energy liberation in a condensed medium occurs volumetrically. Under the combined influence of the volumetric absorption of laser radiation and energy, liberated by the flow of matter through interphase boundaries in both fractions of the target (liquid and solid), conditions are created for the formation of surface temperature maximums and the appearance of very overheated metastable states.

General Processes

Part of the phenomena in a condensed and gaseous medium, independently of laser pulse duration, is always present in the consideration. The presence of phase transitions is common to all the influence modes: melting and evaporation, overheated metastable states, and shock waves in a gaseous medium. The mentioned peculiarities are typical for both nano- and pico- femtosecond pulses.

However, in proceeding from long nanosecond pulses to ultrashort pico- and femtosecond pulses not only does the dynamics of phase transitions and metastable states change, but also the appearance of new phenomena (shock waves in the solid phase and plasma formation processes in evaporated matter or a gaseous medium) occurs. The appearance of low-temperature thermal origin plasma ($5 \times 10^3 < T_{max} < 10^4$ K) occurs after the end of the laser pulse. It is conditioned by forces of gas-dynamic compression and it is connected with the propagation of an intensive shock wave, generated by a strong vapor flow.

Condensed Medium

In terms of applications, the dynamics of phase transitions (melting, evaporation) and peculiarities of their behavior in their dependence on the duration of a laser pulse are of the greatest interest. A decrease in the duration of a laser pulse at the same energy density is accompanied by an increase of the heating rate and correspondingly by an increase in the velocity v_{sl}; and, as is well-known [32], when $t \longrightarrow 0$, the melting front speed $v_{sl} \sim t^{-1/2} \longrightarrow \infty$. However, the real melting rate always remains a finite magnitude. One of the effective mechanisms of restricting the velocity v_{sl} is the hydrodynamics of melt [33]. Its influence becomes apparent particularly in the dependence of the melting temperature $T_m = T_m(P_s)$ on pressure on the melting surface P_s, whose magnitude is defined by the value of the velocity v_{sl}. As a result, an increasing in v_{st} leads to an increase in the pressure P_s and the temperature on the interphase boundary $T_{sl} = T_m(P_s)$, and an increase in the melting temperature $T_m = T_m(P_s)$ restricts the growth of the velocity v_{sl}.

The contribution of overheated metastable states increases with a decrease of τ and it defines the dynamics of phase transitions in many respects. Figure 2 shows a typical example of the spatial structure of the solution at ultrashort $\tau = 10$ fs and $J = 1$ J/cm^2 of the influence in the moment of formation of shock waves in the solid phase and gaseous medium $t \approx 80$ fs.

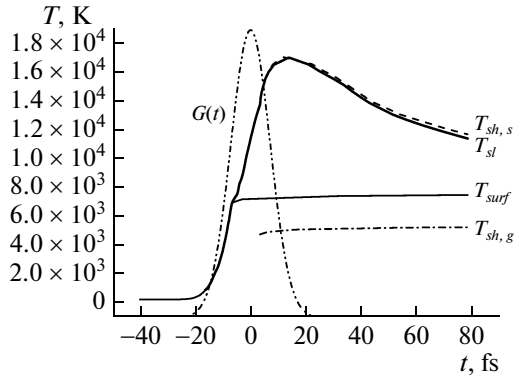

Fig. 3. Temporal profiles of the temperatures T_{sl}, T_{surf}, $T_{sh,\,s}$, and $T_{sh,\,g}$ at the initial moments of time for laser pulse in the influence mode with $\tau = 10$ fs and $G_0 = 10^{15}$ W/cm^2.

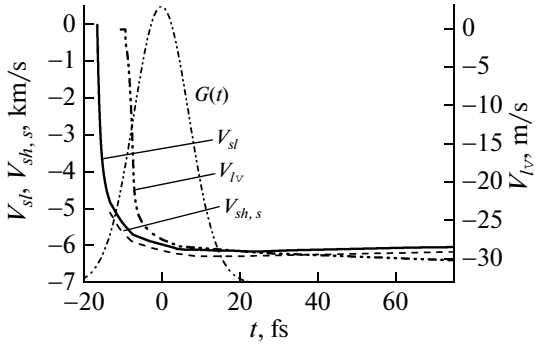

Fig. 4. Temporal profiles of the speed of a melting front v_{sl}, shock wave $v_{sh,\,s}$, and evaporation front v_{lv} for a laser pulse in the influence mode with $\tau = 10$ fs and $G_0 = 10^{15}$ W/cm^2.

The moment of melting of the formation was defined by the heating of the target surface to the equilibrium melting temperature $T_{m,\,0}$. When it was reached, the liquid phase with an initial thickness ~(0.2–2) Å was introduced into consideration. The volumetric mechanism of radiation absorption and the flow of matter through the interphase boundary $x = \Gamma_{sl}$ form the maximum of the surface temperature in the solid phase.

With further heating of the target surface to the temperature, at which the pressure of the saturated vapor on the liquid surface begins exceeding air pressure, the second phase transition, surface evaporation, is introduced into consideration. Intensive surface evaporation combined with the liberation of volumetric energy of laser radiation form the second surface temperature maximum (Fig. 2) in liquid at some distance from the evaporation front. The position of the temperature maximums in solid and liquid phases is defined by the correlation of phase front's motion speeds and coefficients of thermal diffusivity and absorption [17]. Since maximal values of the velocities v_{sl} and v_{lv} fit the expression $v_{sl} \gg v_{lv}$ (Fig. 3), the value of the temperature maximum in a solid body considerably exceeds that of liquid.

The main peculiarity of threshold modes for ablation $\tau < 10^{-10}$ s and $0.1 < J <$ J/cm^2 consists of the fact that the thickness of the liquid phase doesn't exceed 100–200 Å and it is transparent for laser radiation. The energy of the laser pulse is almost completely absorbed in the solid phase, causing its considerable overheating ($T_{s,\,\max} \sim 2000$ K). The accumulated energy is mainly spent on the heating and melting of the solid phase. Therefore, the melting process occurs more efficiently and the role of evaporation at low energy densities $0.1 < J$ 1 J/cm^2 is negligible. For the intensification of the ablation process in the picosecond range, it is necessary to increase the density of the absorbed energy to $J > 1$ J/cm^2.

In the ultrashort pulse range ($10^{-12} < \tau \le 10^{-15}$) at $1 \le J \le 10$ J/cm^2, the rapid heating of the target, the high melting rate, and relatively slow energy transfer at the expense of thermal conductivity lead to a significantly stronger overheating of the solid phase in comparison with long nanosecond pulses. The maximal melting front speed at $T \approx 10^{-13}$–10^{-15} s reaches acoustic speed in a solid body, which constitutes ~6.26×10^5 cm/s for aluminium. The approximation of the velocity v_{sl} to acoustic speed, on the one hand, creates conditions for the appearance of a shock wave in the solid phase and, on the other hand, it promotes its maximal overheating (Fig. 2). At the moment of the formation of shock waves in gaseous and solid phases $t \approx 80$ fs, the temperature maximum in the solid phase at $\tau = 10$ fs and $J = 1$ L/cm^2 is located at a depth of ~200 Å from the boundary $\Gamma_{sl}(t)$ and it constitutes ~6×10^3 K. The degree of overheating degree $T_{s,\,\max}/T_{m0}$ reaches a value of ~6.5. Correspondingly, the velocity, temperature, and pressure on the interphase boundary $\Gamma_{sl}(t)$ equal to $v_{sl} = 4 \times 10^3$ ms^{-1}, $T_{sl} \gg T_{m0} = 1.5 \times 10^3$ K, and $P_s \approx 0.5$ Mbar. The mentioned pressures are sufficient for the excitation of a strong shock wave in the solid phase.

Increasing the energy density to $J = 10$ J/cm^2 at the same duration leads to a sharp intensification of all overheating parameters (Fig. 3). Figures 3 and 4 show temporal involutions of the temperature on the interphase boundaries $T_{surf}(t)$ and $T_{sl}(t)$ and on the front of the shock waves $T_{sh,\,s}(t)$ and $T_{sh,\,g}(t)$, and also on their corresponding propagation velocities $v_{sl}(t)$, $v_{lv}(t)$, and $v_{sh}(t)$. The curves imply that phase transitions and the shock wave in the solid phase appear on the rising edge of the laser pulse. Towards the middle of the pulse, the velocity of the front reaches its limiting value, which is equal to the acoustic speed.

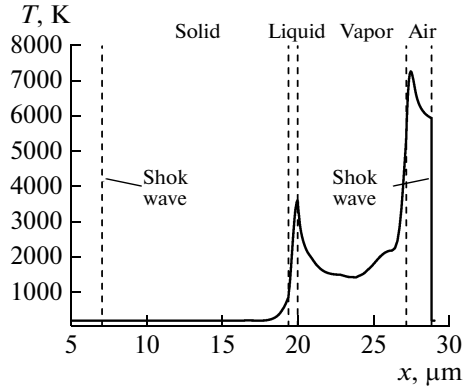

Fig. 5. Spatial temperature profile at the moment $t = 2.5$ ns in the influence mode with $\tau = 10$ fs and $G_0 = 10^{15}$ W/cm^2.

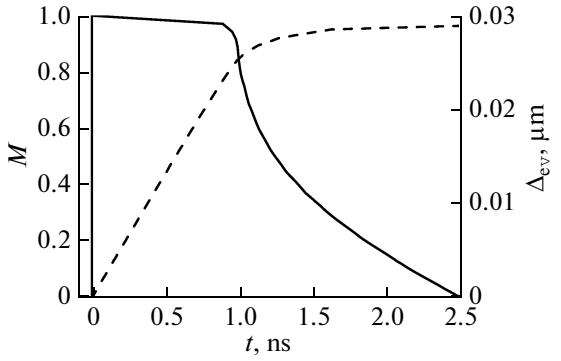

Fig. 6. Temporal profiles of the evaporation rate in terms of Mach numbers on the external side of the Knudsen layer and the thickness of the evaporated layer in the influence mode with $\tau = 10$ fs and $G_0 = 10^{15}$ W/cm^2.

The melting front and shock wave front possess approximately the same velocities and temperatures and they propagate as a single complex. The energy accumulated in the solid phase provides a stabilizing influence on the temperature of the evaporated surface, which reaches a magnitude of $T_{surf} = 7 \times 10^3$ K and remains constant till the complete disappearance of the overheating. The propagation velocities of the shock waves and phase fronts also remain constant (Fig. 4). At the moment $t \approx 2.5 \times 10^{-8}$ s, the excess energy is completely removed from the overheating region and the spatial distribution of temperature no longer contains surface maximums (Fig. 5). Such a lengthy energy redistribution in comparison with the duration of the laser pulse is defined by the domination of the relatively slow conductive transfer mechanism. It is precisely the slow energy redistribution that explains the large thicknesses of the molten and removed material. Thus, the melting front during the time $t \approx 0.5 \times 10^{-8}$ s after the end of the laser pulse moves at the acoustic speed together with the shock wave front. In time, with a decrease of the temperature gradients in the interphase region, the velocity v_{sl} decreases and the single complex of melting fronts and the shock wave disintegrates. The shock wave becomes attenuated and its front goes far forward at the acoustic speed (Fig. 5).

Surface evaporation before $t = 0.8 \times 10^{-8}$ s occurs with the maximum possible velocity, the Mach number on the external boundary of the Knudsen layer $M = 1$ (Fig. 6). By the moment $t = 0.8 \times 10^{-8}$ s, plasmic formations begin appearing in the gaseous medium under the influence of gas-dynamic compression forces, whose pressure exceeds the pressure of saturated vapor, and this slows down the evaporated matter flow. The Mach number constantly decreases and by the moment $t \approx 2.5 \times 10^{-8}$ it reduces to zero, $M = 0$ (Fig. 6); formally this corresponds to the end of the evaporation process. Evaporation stops despite the fact that the surface temperature at this moment $T_{surf} = 3700$ K exceeds the equilibrium boiling temperature of aluminium $T_b = 2730$ K.

Approximately the same process pattern is observed in the picosecond influence range; this is testified by the spatial distribution of the temperature at the moment $t \approx 2.5 \times 10^{-8}$ s (Fig. 7). A comparatively small amount of liquid manages to appear during the influence of the laser pulse in the considered duration range. The thickness of the liquid phase during the pulse influence doesn't exceed 300 Å. It is almost transparent for laser radiation because of the bleaching in the transcritical region. As a result, an almost spatially constant temperature is established in the liquid $T_{sl} \approx T_{lv}$. After the end of the influence of the pulse, the accumulated overheating energy of the solid phase is spent on heating the liquid phase and maintaining a high surface temperature. This ensures the long duration of the melting and evaporation processes in comparison with the duration of the laser pulse.

Since the energy transfer from the heated solid phase region into the liquid phase is performed by a relatively slow thermal conductivity mechanism, the typical time of phase transformations for pico- and femtosecond pulses turn out to be approximately the same and is $t = 2.5$–3.0 ns (Fig. 8). Surface temperature maximums completely disappear by the moment $t \sim 2.0$–2.2 ns (Figs. 3, 7).

The dynamics of the considered phase transitions undergoes essential changes with a change of the duration of laser pulses. Figures 9 and 10 show the dependences of the maximal values of the melting rate v_{sl}, evaporation rate v_{lv}, thicknesses of melt Δ_l, and evaporated layers Δ_{ev} on the duration of laser pulses. Analysis of these dependences showed that in long pulses $10^{-8} \geq \tau \geq 10^{-9}$ s and energy density $1 \leq J \leq 10$ J/cm^2, melting and evaporation occur according to the usual scheme. The surface temperature

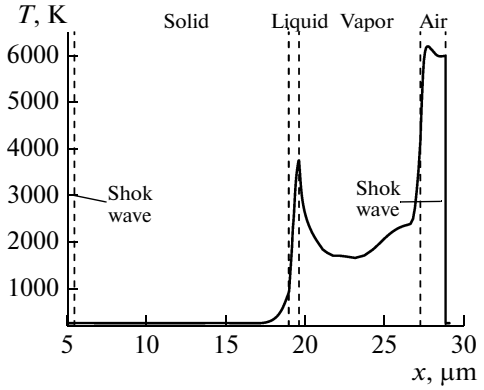

Fig. 7. Spatial temperature profile at the moment $t = 2.5$ ns in the influence mode with $\tau = 1.0$ ps and $G_0 = 10^{13}$ W/cm^2.

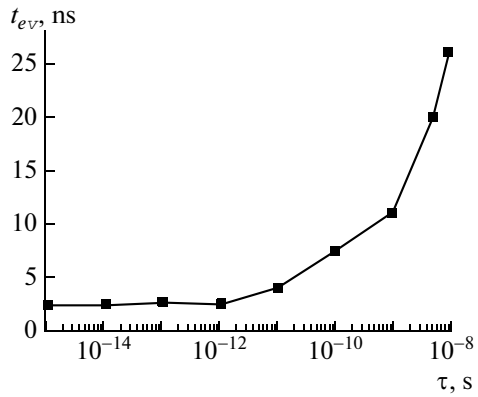

Fig. 8. Dependence of the duration of evaporation on the duration of the influencing pulse.

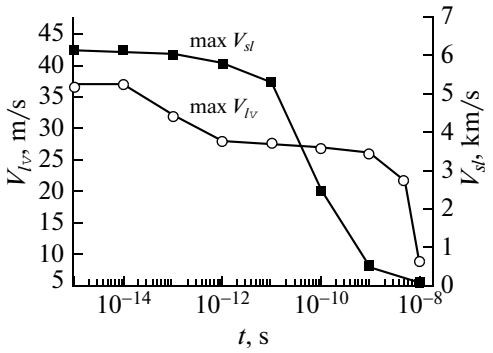

Fig. 9. Dependences of maximal values of melting $v_{sl}(\tau)$ and evaporation $v_{lv}(\tau)$ rates on laser pulse duration τ.

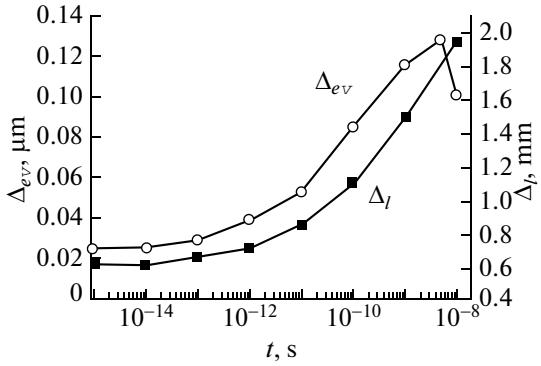

Fig. 10. Dependences of the thicknesses of the melt $\Delta_l(\tau)$ and the evaporated layer $\Delta_{ev}(\tau)$ on laser pulse duration τ.

$T_{sur} \approx (5.7–7.2) \times 10^3$ K and the surface evaporation rate $|v_{lv}| = 10–27$ m s^{-1} follow the change of the radiation intensity with a little delay. Values of the maximal melting rate are contained in the range $50–5 \times 10^2$ m s^{-1} (Fig. 9). The maximal melt thickness grows with an increase of τ and reaches its maximum at $\tau = 10^{-8}$ s, ($\delta_{liq} \approx 1.9$ μm) (see Fig. 10).The thickness of the removed material Δ_{ev} is greater than Δ_l by more than one order of magnitude (Fig. 10). Pressure on the surface of the solid phase P_s doesn't exceed 4×10^3 bar. The temperature T_{sl} on the interphase boundary at such pressure barely differs from the equilibrium temperature $T_{sl} \cong T_{m0}$. Surface a temperature maximum is at some distance from the interphase boundary Γ_{sl} and its value exceeds that of equilibrium melting temperature by several tens of degrees. Such negligible overheating of the solid phase disappears relatively fast without qualitatively affecting the melting and evaporation processes. Its presence influences only the increase of the life time of the melt and the duration of the evaporation process, which turns out to be 2.5 times greater than the duration τ at $\tau \cong 10^{-8}$ s (Fig. 8).

Temporal dependences of the maximal melt depth $\Delta_l(\tau)$ of the evaporated layers $\Delta_{ev}(\tau)$ tend to decrease with a decrease of τ and they change in the range $\Delta_l(\tau) \sim (1.95–0.6)$ μm and $\Delta_{ev}(\tau) \sim (0.13$ μm$–230$ Å) (see Fig. 4). It is necessary to note that the thickness of the evaporated matter is in good agreement with the experimental data [15]. Thus, owing to the appearance of overheated metastable states, a decrease of the duration of the laser pulse by 4–7 orders of magnitude leads to a decrease of the thicknesses $\Delta_l(\tau)$ and $\Delta_{ev}(\tau)$ by only 3–6 times. According to the expression $v_{sl} \gg v_{lv}$ (Fig. 9), the melt depth $\Delta_l(\tau)$ in all the considered time span turns out to be much greater than the thickness of the evaporated layer $\Delta_{ev}(\tau)$ and their relation is equal to $\Delta_l(\tau)/\Delta_{ev}(\tau) \approx 10–30$ (Fig. 10). However, in the femtosecond range, where the temperature of metastable states approximates the critical temperature or exceeds it, one should most probably expect the surface evaporation mechanism to be changed by a volumetric one.

Gaseous Medium

The state of the vapor near the liquid boundary in the mode before the plasma is mainly defined by the temperature on the evaporating surface and the thermal conductivity of the liquid. At the same time, the heating of vapor due to the absorption of the laser radiation, for which it is almost transparent, is negligible.

In a gaseous medium, a fast expanding vapor flow, whose speed near the contact boundary reaches several kilometers per second, acts like an accelerating piston, pushing cold air out. Beginning from a certain moment of time, it leads to the formation of a shock wave in the gas. The shock wave, explicitly distinguished with the help of the Rankin–Hugoniot conditions, propagates towards the laser radiation. Significantly later, after the end of the influence of the laser, a low-temperature plasma appears in the gaseous phase due to the work of the compression forces.

Figure 2 shows a typical example of the structure of a spatial solution, obtained during an ultrashort ($\tau = 10$ fs) influence at the moment of the developed plasma formation, $t \approx 2.5$ ns. The maximal plasma temperature reaches a magnitude of $T_{\max} \approx 7400$ K and it is located behind the shock wave front near the vapor-air contact boundary. The spatial size of the vapor domain during the influence of the pulse is small and it constitutes $\sim 7 \times 10^{-3}$ μm, and by the end of evaporation it reaches a magnitude of 7.5 μm (Fig. 5).

At a high enough intensity of laser radiation $G > 10^{16}$ W/cm^2 in vapor near the evaporating surface, laser plasma may appear, starting with the avalanche-like growth of temperature, the concentration of charged particles, and the absorption coefficient. This process of strongly ionized and absorbing plasma is an equilibrium analogue of the optical breakdown. The vapor temperature sharply increases to 10^6 K, the concentration of electrons $N_e \approx 8 \times 10^{22}$ cm^{-3}, and the absorption coefficient $\kappa \approx 10^5$ cm^{-1}. A new shock wave is formed, which propagates from the surface, catches up with the first shock wave in the gas and absorbs it. A decrease of the laser energy flow on the target surface, caused by the growth of the absorption coefficient with a simultaneous increase of the pressure in the plasma, leads to a complete stopping of the surface evaporation.

CONCLUSIONS

The performed analysis allows one to conclude that long nanosecond and ultrashort pico- and femtosecond pulses essentially differ from each other by mechanisms of the transformation of the energy of laser pulses at one and the same energy density J.

For long pulses of $\tau \sim 10$ ns, the maximal value of the surface temperature ($T_{sur} \approx 5800$ K) is reached with a negligible displacement with respect to the peak pulse intensity. A slight overheating of the solid phase (tens of degrees) promotes an increase of the evaporation time t_{vap} by 2.5 times with respect to the duration of the laser pulse τ. Most of the energy of the pulse is spent on melting and evaporation processes. A smaller part of the energy is spent on heating the solid phase and generation of a shock wave in a gaseous medium.

In proceeding to ultrashort pulses, an increasing part of the energy of laser pulses is spent on creating overheated metastable states in a condensed medium and generating shock waves in a solid phase and in a gaseous medium. Less part of energy is spent on evaporation process. Thus, if at $\tau \sim 10$ ns, the relation of the thicknesses $\Delta_l(\tau)/\Delta_{\text{ev}}(\tau)$ did not exceed 20, then at $\tau \sim 10$ fs it reaches 30.

In the femtosecond range, the magnitude of the overheating of the solid phase $T_{s,\max}/T_{m0}$ reaches the values 8–10, and the maximum surface temperature becomes comparable with the critical temperature. In these cases, the spinodal decomposition of metastable states or the nucleation of a new phase are very likely to occur; this corresponds to a change of the surface mechanisms of phase transformations by volumetric ones.

ACKNOWLEDGMENTS

This study was supported by the Russian Foundation for Basic Research, projects no. 09-01-12110-ofi_m, 09-07-00225.

REFERENCES

1. W. W. Duley, *UV Lasers: Effects and Applications in Materials Science* (University Press, Cambridge, 1996).
2. V. I. Mazhukin and A.A. Samarskii, "Mathematical Modeling in the Technology of Laser Treatments of Materials. Review," Surv. Math. Industry **4** (2), 85–149 (1994).
3. K. Sokolowski-Tinten and D. von der Linde, "Generation of Dense Electron-Hole Plasmas in Silicon," Phys. Rev. B **61**, 2643–2650 (2000).

4. V. M. Gordienko, M. S. Dzhidzhoev, V. V. Kolchin, S. A. Magnitskii, V. T. Platonenko, A. B. Savel'ev, and A. P. Tarasevich, "On the Problem Whether it is Possible to Generate Pico- and Subpicosecond X-ray Pulses in Thin Films," Kvant. Elektron. **22** (2), 158–160 (1995).
5. *Laser Ablation. Principles and Applications,* J. C. Miller, Ed., (Springer, Berlin, 1994).
6. A. A. Vedenov and G. G. Gladush, *Physical Processes under Materials Laser Processing* (Energoatomizdat, Moscow, 1985) [in Russian].
7. A. A. Samokhin, "Effect of Laser Radiation onto Absorbing Condensing Mediums," Trudy IOFAN **13**, 1–119 (1988).
8. V. I. Mazhukin, M. G. Lobok, and I. Smurov, "Transient Effects in Pulsed Laser Irradiation," Appl. Surf. Sci. **253**, 7744–7748 (2007).
9. G. P. Pinho, H. Schittenhelm, W. W. Duley, S. A. Schueter, H. R. Jamani, and R. E. Mueller, "Energy Distributions in the Laser Ablation of Metals and Polymers," Appl. Surf. Sci. **127–129**, 983–987 (1998).
10. V. I. Mazhukin, V. V. Nossov, and I. Smurov, "Modeling of Plasma-Controlled Evaporation and Surface Condensation of Al Induced de 1.06 and 0.248 μm Laser Radiations, Appl. Phys. **101** (2), 24922–24937 (2007).
11. A. Peterlongo, A. Miotello, and R. Kelly, "Laser-Pulse Sputtering of Aluminum: Vaporization, Boiling Superheating, and Gas-Dynamic Effects," Phys. Rev. **50** (6), 4716–4727 (1994).
12. D. von der Linde, "A Picosecond View of Melting," Science **302**, 1345–1346 (2003).
13. H. Iglev, M. Schmeisser, K. Simeonidis, A. Thaller, and A. Laubereau, "Ultrafast Superheating and Melting of Bulk Ice," Nature **439**, 183–186 (2006).
14. B. N. Chichkov, C. Momma, S. Nolte, F. von Alvensleben, and A. Tunnermann, "Precise Deep Drilling of Metals by Femtosecond Laser Pulses," Appl. Phys. A **63**, 105–109 (1996).
15. M. D. Shirk and P. A. Molian, "A Review of Ultrashort Pulsed Laser Ablation of Materials," J. Laser App. **10**, No. 1, 18–28 (1998).
16. K. Sokolowski-Tinten and D. von der Linde. "Ultrafast Phase Transitions and Lattice Dynamics Probed Using Laser-Produced X-ray Pulses," J. Phys. Cond. Mat. **16**, R1517–R1536 (2004).
17. D. Boschetto, E. G. Gamaly, A. V. Rode, B. Luther-Davies, D. Glijer, T. Garl, O. Albert, A. Rousse, and J. Etchepare, "Small Atomic Displacements Recorder in Bismuth by the Optical Reflectivity of Femtosecond Laser-Pulse Excitations," Phys. Rev. Lett. **100**, 027404-1–027404-4 (2008).
18. E. G. Gamaly, A. V. Rode, V. T. Tikhonchuk, and B. Luther-Davies, "Ablation of Solids by Femtosecond Lasers: Ablation Mechanism and Ablation Thresholds for Metals and Dielectrics," Phys. Plasmas **9**, 949–957 (2002).
19. Zh. Lin and L.V. Zhigilei, "Thermal Excitation of d Band Electrons in Au: Implications for Laser-Induced Phase Transformations," Proc. of SPIE **6261**, 62610U-1–62610U-10 (2006).
20. Zh. I. Alferov, Yu. V. Koval'chuk, Yu. I. Pogorel'skii, and O. V. Smol'skii, "Picosecond Laser Pulses Impacts onto Si to the Compounds Semiconductor of A^3V^5," Izv. Akad. Nauk SSSR, Ser. Fiz. **49** (6), 1069–1075 (1985).
21. X. Xu, C. Grigoropoulos, and R. E. Russo, "Measurements of Solid/Liquid Interface Temperature During Pulsed Excimer Laser Melting of Polysilicon Films," Appl. Phys. Lett. **65** (14), 1745–1747 (1994).
22. V. I. Mazhukin, I. Smurov, G. Flamant, and C. Dupuy, "Peculiarities of Laser Melting and Evaporation of Superconducting Ceramics," J. Thin Solid Films **241**, 109–113 (1994).
23. V. I. Mazhukin, I. Smurov, and G. Flamant, "Overheated Metastable States in Pulsed Laser Action on Ceramics," J. Appl. Phys. **78** (2), 1259–1270 (1995).
24. S. Williamson, C. Mourou, and J. C. H. Li, "Time-Resolved Laser-Induced Phase Transformation in Aluminum," Phys. Rev. Lett. **52** (26), 2364–2368 (1984).
25. M. Kandyla, T. Shih, and E. Mazur, "Femtosecond Dynamics of the Laser-Induced Solid-to-Liquid Phase Transition in Aluminum," Phys. Rev. B **75**, 214107–214132 (2007).
26. D. S. Ivanov and L. V. Zhigilei, "Combined Atomistic–Continuum Modeling of Short-Pulse Laser Melting and Disintegration of Metal Films," Phys. Rev. B **68**, 064114-1–064114-21 (2003).
27. D. S. Ivanov and L. V. Zhigilei, "Channels of Energy Registribution in Short-Pulse Laser Interactions with Metal Targets," Appl. Surf. Sci. **248**, 433–439 (2005).
28. V. I. Mazhukin, P. A. Prudkovskii, and A. A. Samokhin, "On Gasdynamics Boundary Conditions on Evaporation Front," Mat. Model. **5** (6), 3–10 (1993).
29. J. Lees and B. H. J. Williamson, "Combined Very High Pressure/High Temperature Calibration of the Tetrahedral Anvil Apparatus, Fusion Curves of Zinc, Aluminum, Germanium and Silicon to 60 Kilobars," Nature, Phys. **208** (5007), T84–T85 (1965).
30. K. S. Holian., "A New Equation of State for Aluminum," J. Appl. Phys. **59** (1), 149–157 (1986).
31. P. V. Breslavskii and V. I. Mazhukin, "Dynamically Adapted Grids for Interacting Discontinuous Solutions," Zh. Vychisl. Mat. Mat. Fiz. **47** (4), 717–737 (2007) [Comput. Math. Math. Phys. **47** (4), 687 (2007)].
32. H. S. Carslaw and J. C. Jaeger, *Conduction of Heat in Solids* (Oxford Univ. Press, 1959; Nauka, Moscow, 1964).
33. P. V. Breslavskii, V. I. Mazhukin, and A. A. Samokhin, "On Hydrodynamic Variant for Calculating the Stephan's Problem for the Substance Being in Metabolic State," Dokl. Akad. Nauk SSSR **320** (5), 1088–1092 (1991).